Lecture 6 (21.10.2020)

Nanomechanical Measurements

I. Displacement Measurement

I now want to discuss measurements of nanomechanical displacements. Nanomechanical elements are typically transducers, i.e. devices that convert force, torque, mass change, etc. into a displacement or phase shift. This displacement or phase shift then has to be measured by a detector. Such detectors of nanomechanical motion are typically optical or electronic. Together the transducer and the detector make the force, torque, or mass change sensor.

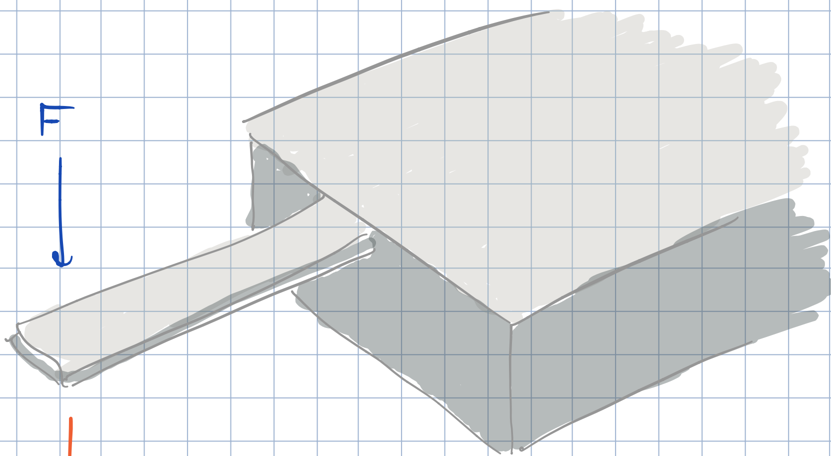

$F = kx$

Transducer of F into x.

Now displacement x must be detected by:

- tunneling
- optical deflection
- optical interferometry
- microwave interferometry
- magnetomotive effect
- piezoelectric effect
- capacitive effect

Displacement Measurements

, NUMBER 9 PHYSICAL REVIEW LETTERS 3 M

Atomic Force Microscope

G. Binnig[(a)] and C. F. Quate[(b)]
Edward L. Ginzton Laboratory, Stanford University, Stanford, California 94305

and

Ch. Gerber[(c)]
IBM San Jose Research Laboratory, San Jose, California 95193

(Received 5 December 1985)

The scanning tunneling microscope is proposed as a method to measure forces as small as 10^{-18} N. As one application for this concept, we introduce a new type of microscope capable of investigating surfaces of insulators on an atomic scale. The atomic force microscope is a combination of the principles of the scanning tunneling microscope and the stylus profilometer. It incorporates a probe that does not damage the surface. Our preliminary results *in air* demonstrate a lateral resolution of 30 Å and a vertical resolution less than 1 Å.

STM Detection

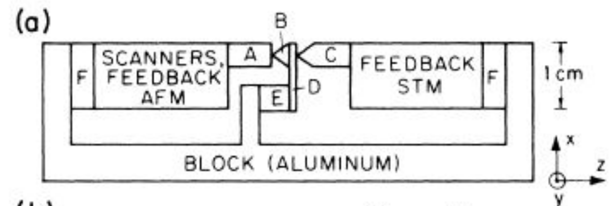

(b)

A: AFM SAMPLE
B: AFM DIAMOND TIP
C: STM TIP (Au)
D: CANTILEVER, STM SAMPLE
E: MODULATING PIEZO
F: VITON

Displacement Measurements

Novel optical approach to atomic force microscopy

Gerhard Meyer and Nabil M. Amer[a]
IBM Thomas J. Watson Research Center, Yorktown Heights, New York 10598

(Received 21 April 1988; accepted for publication 11 July 1988)

A sensitive and simple optical method for detecting the cantilever deflection in atomic force microscopy is described. The method was incorporated in an atomic force microscope, and imaging and force measurements, in ultrahigh vacuum, were successfully performed.

Laser deflection

An atomic-resolution atomic-force microscope implemented using an optical lever

S. Alexander,[a] L. Hellemans, O. Marti,[b] J. Schneir,[c] V. Elings, and P. K. Hansma
Department of Physics, University of California, Santa Barbara, California 93106
Matt Longmire and John Gurley
Digitial Instruments, Inc., 135 Nogal Drive, Santa Barbara, California 93110

(Received 7 July 1988; accepted for publication 14 September 1988)

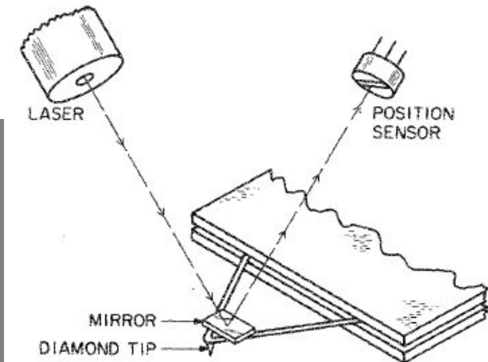

FIG. 1. The cantilever deflection detection scheme. The cantilever is 1.4 mm long, and the distance from the mirror to the position sensor is 10 cm.

Displacement Measurements

Laser interferometry

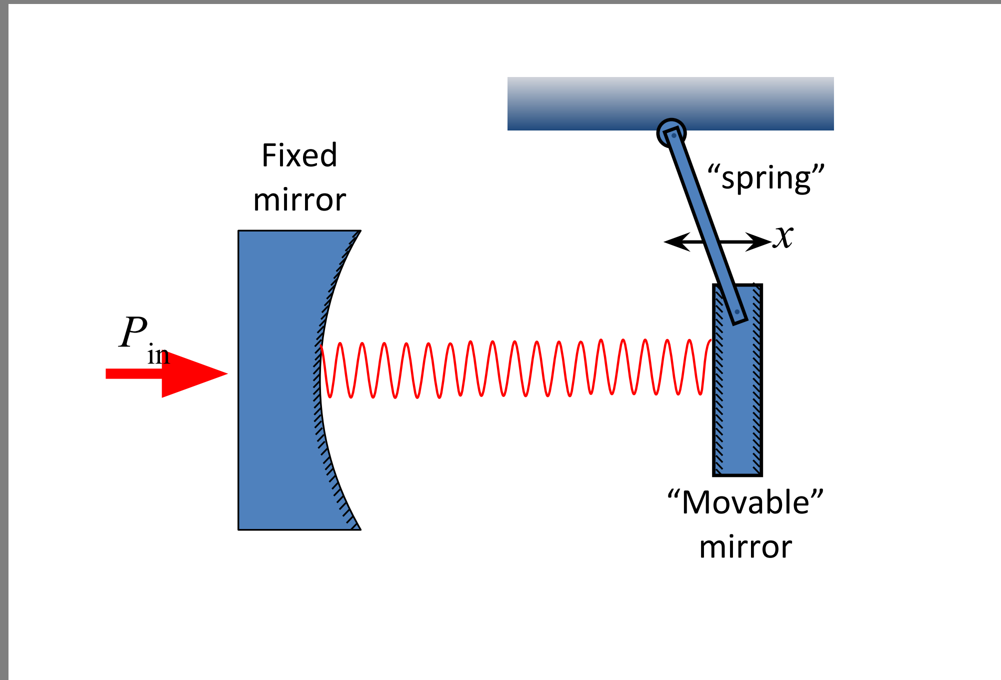

Displacement Measurements

Laser interferometry

QUANTUM OPTICS AND PRECISION MEASUREMENTS, APPLICATIONS TO GRAVITATIONAL EXPERIMENTS

Ultrasensitive Optical Measurement of Thermal and Quantum Noises[1]

T. Caniard, T. Briant, P.-F. Cohadon, M. Pinard, and A. Heidmann

Laboratoire Kastler Brossel, Case 74, F75252 Paris Cedex 05, France

e-mail: caniard@spectro.iussieu.fr; briant@spectro.jussieu.fr; cohadon@spectro.jussieu.fr; pinard@spectro.jussieu.fr; heidmann@spectro.jussieu.fr

Received October 12, 2006

Abstract—We have developed an experiment of ultrasensitive interferometric measurement of small displacements based on a high-finesse Fabry–Perot cavity. We have observed the internal thermal noise of mirrors and fully characterized their acoustics modes with a sensitivity of 3×10^{-20} m/Hz$^{1/2}$. This unique sensitivity is a step towards the first observation of the radiation pressure effects and the resulting standard quantum limit in interferometric measurements. Our experiment may become a powerful facility to test quantum noise reduction schemes such as the use of squeezed light or quantum locking of mirrors. As a first result, we present the observation of a cancellation of radiation pressure effects in our cavity. This back-action noise cancellation was first proposed within the framework of gravitational-wave detection with dual resonators, and may drastically improve the sensitivity of such measurements.

Displacement Measurements

Laser interferometry

LIGO – Gravitational Wave Detection

Displacement Measurements

Force microscope using a fiber-optic displacement sensor

D. Rugar, H. J. Mamin, R. Erlandsson,[a] J. E. Stern, and B. D. Terris

IBM Research Division, Almaden Research Center, 650 Harry Road, San Jose, California 95120-6099

(Received 1 June 1988; accepted for publication 27 July 1988)

A force microscope is described which uses a fiber-optic interferometer as the cantilever displacement sensor. Low thermal drift and reduced susceptibility to laser frequency variation are achieved due to the small (several micrometer) size of the interferometer cavity. A sensitivity of 1.7×10^{-4} Å/$\sqrt{\text{Hz}}$ is observed for frequencies above 2 kHz. The drift rate of the sensor is on the order of 3 Å/min. As an initial demonstration, laser-written magnetic domains in a thin film sample of TbFeCo were imaged.

$$10^{-13} m/\sqrt{Hz}$$

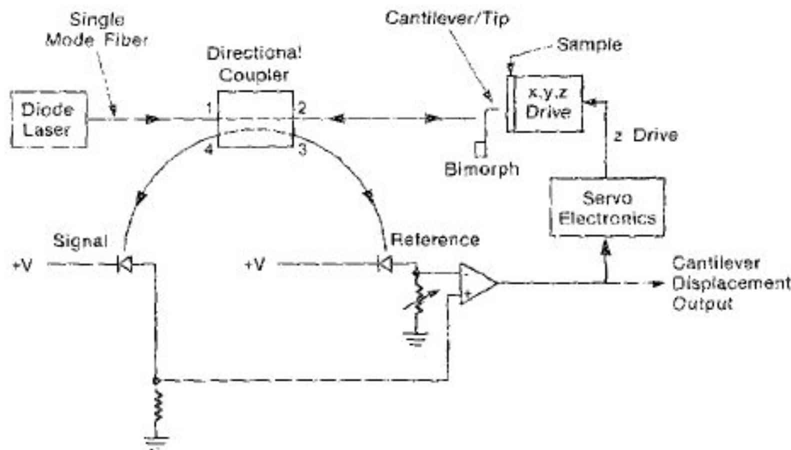

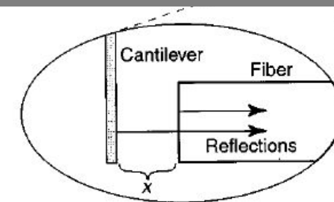

FIG. 1. Schematic diagram of the interferometer.

Laser interferometry

Displacement Measurements

Microwave interferometry – capacitive detection

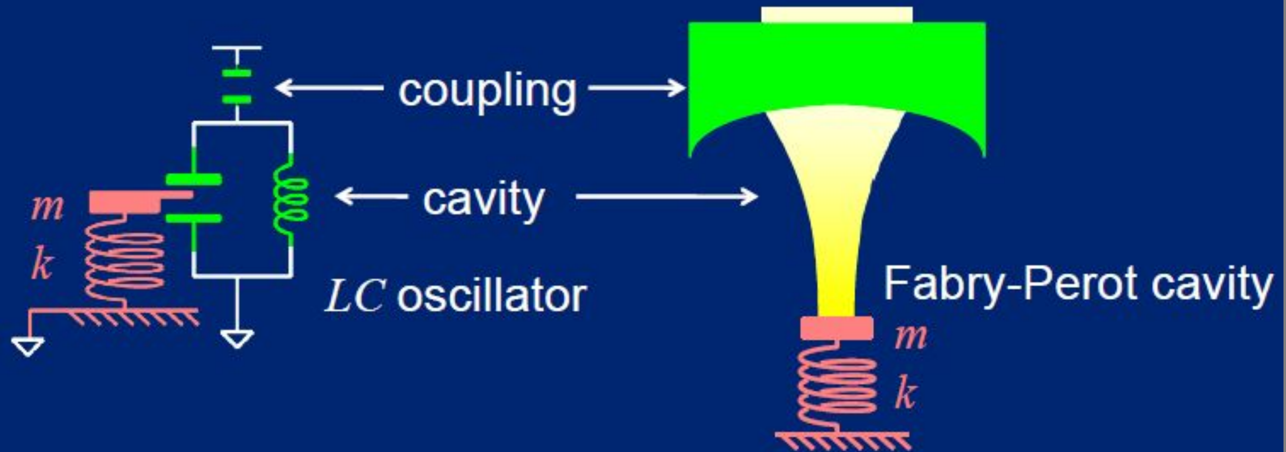

K. L. Lehnert, JILA

Displacement Measurements

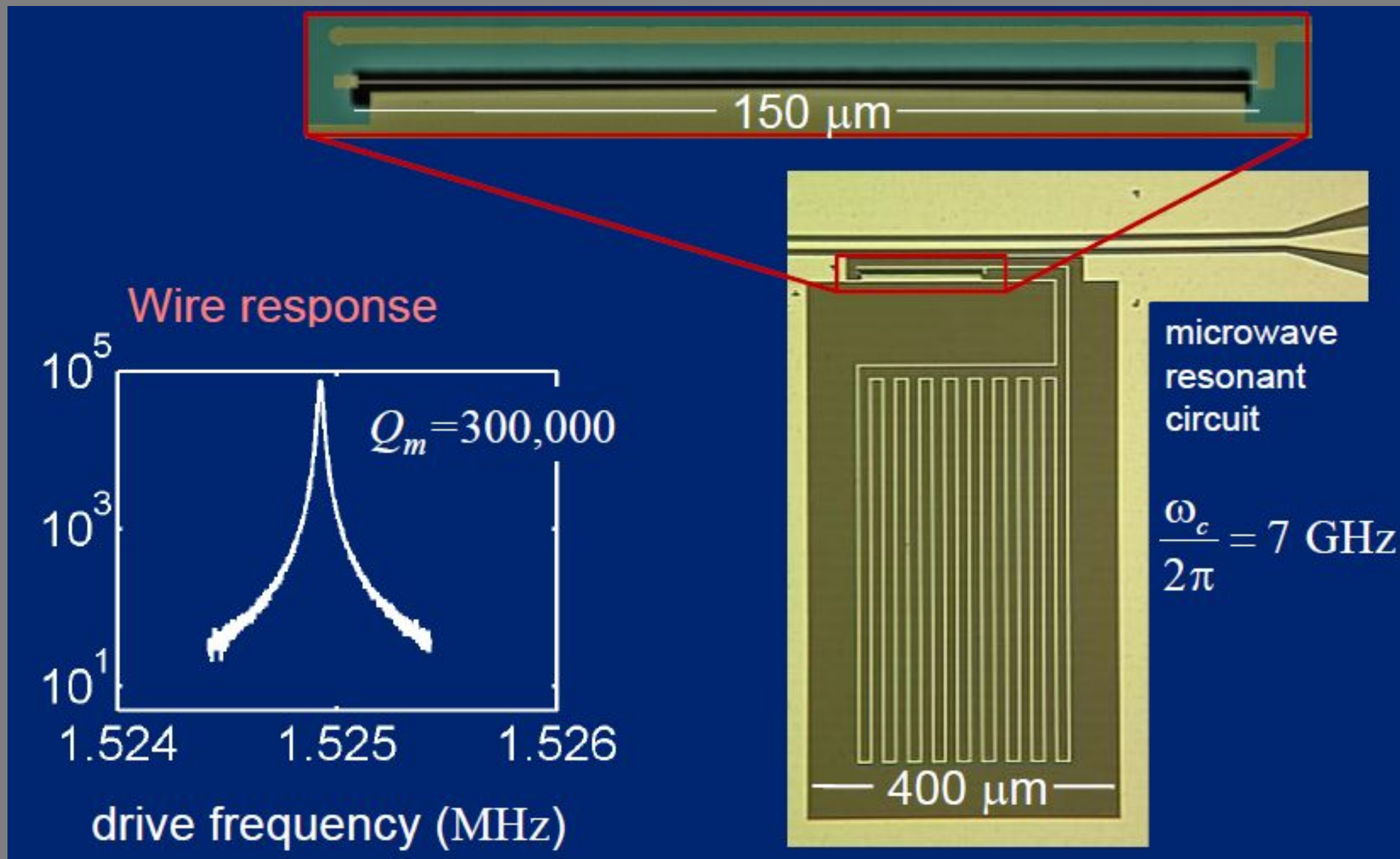

$10^{-15} m/\sqrt{Hz}$

K. L. Lehnert, JILA

Displacement Measurements

Magnetomotive detection (via Faraday's Law)

$$\textbf{EMF generated} \propto \frac{d\Phi}{dt}$$

$$V_{EMF}(t) = \zeta L B \dot{x}$$

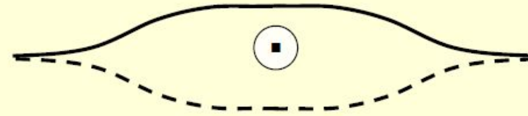

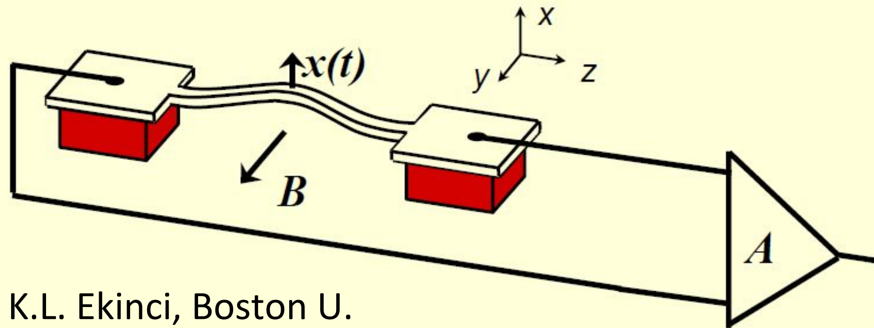

Figure from K.L. Ekinci, Boston U.

A. Cleland & M. Roukes, 1999.

Displacement Measurements

Nanometre-scale displacement sensing using a single electron transistor

Robert G. Knobel*† & Andrew N. Cleland*

* *Department of Physics and iQUEST, University of California, Santa Barbara, California 93106, USA*

$$10^{-15} m / \sqrt{Hz}$$

Capacitive detection

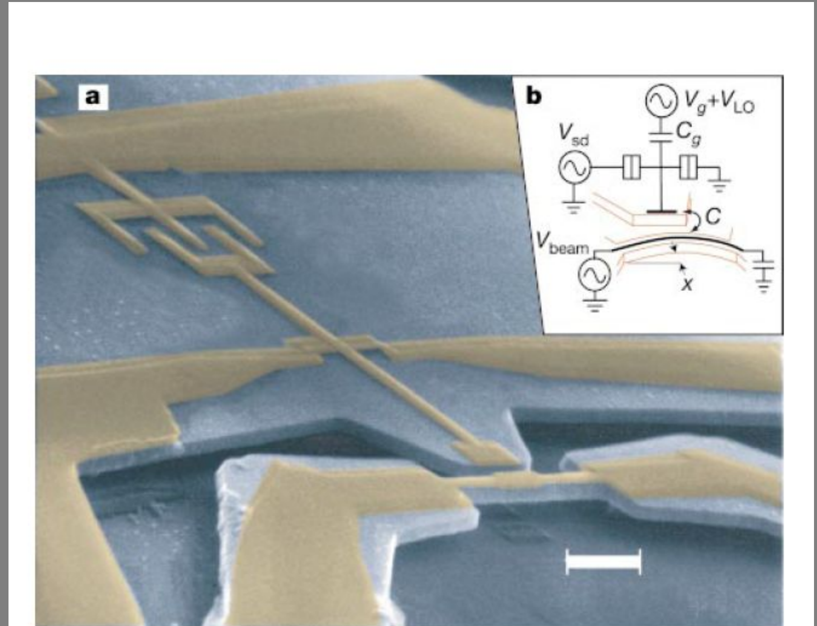

Figure 1 The device used in the experiment. **a**, Scanning electron micrograph of the device, showing the doubly clamped GaAs beam, and the aluminum electrodes (coloured) forming the single electron transistor and beam electrode. Scale bar, 1 μm. The Al/AlO$_x$/Al tunnel junctions have approximately 50 × 50 nm^2 overlap. **b**, A schematic of the mechanical and electrical operation of the device.

Displacement Measurements

Approaching the Quantum Limit of a Nanomechanical Resonator

M. D. LaHaye,[1,2] O. Buu,[1,2] B. Camarota,[1,2] K. C. Schwab[1]*

By coupling a single-electron transistor to a high–quality factor, 19.7-megahertz nanomechanical resonator, we demonstrate position detection approaching that set by the Heisenberg uncertainty principle limit. At millikelvin temperatures, position resolution a factor of 4.3 above the quantum limit is achieved and demonstrates the near-ideal performance of the single-electron transistor as a linear amplifier. We have observed the resonator's thermal motion at temperatures as low as 56 millikelvin, with quantum occupation factors of N_{TH} = 58. The implications of this experiment reach from the ultimate limits of force microscopy to qubit readout for quantum information devices.

Capacitive detection

$$10^{-15} m/\sqrt{Hz}$$

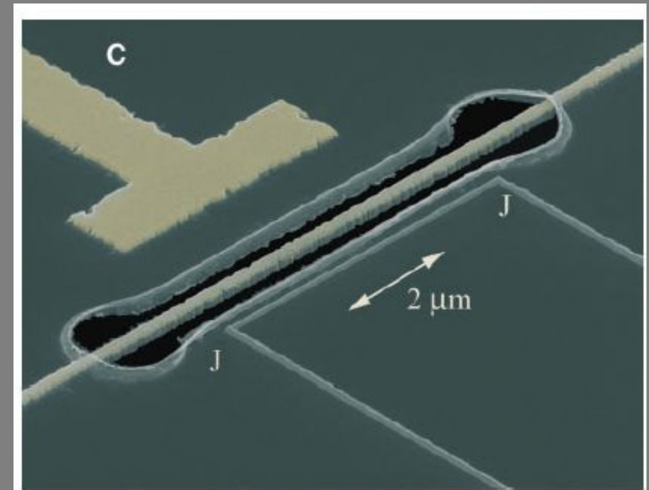

Displacement Measurements

APPLIED PHYSICS LETTERS VOLUME 81, NUMBER 9 26 AUGUST 2002

Nanomechanical displacement sensing using a quantum point contact

A. N. Cleland[a] and J. S. Aldridge
Department of Physics and iQUEST, University of California, Santa Barbara, California, 93106

D. C. Driscoll and A. C. Gossard
Materials Department and iQUEST, University of California, Santa Barbara, California, 93106

Piezoelectric detection

$$3\times10^{-12}\, m/\sqrt{Hz}$$

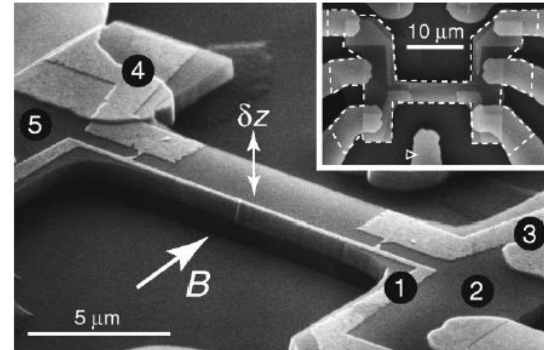

FIG. 1. SEM micrograph of the QPC electrodes defined on the surface of a suspended beam. The magnetic field B used for magnetomotive actuation is indicated, as is the direction of flexure δz. The numbers identify the electrodes: (1) is the drive electrode that also serves as a QPC gate, (2) and (5) define the source and drain ohmic contacts, (3) and (4) the other sides of the two QPC gates. Only one QPC was used at a time. Inset: Larger scale image of the structure, with the dotted line outlining the suspended area.

Displacement Measurements

An off-board quantum point contact as a sensitive detector of cantilever motion

M. POGGIO[1,2]*, M. P. JURA[3], C. L. DEGEN[1], M. A. TOPINKA[4,5], H. J. MAMIN[1], D. GOLDHABER-GORDON[4] AND D. RUGAR[1]

[1]IBM Research Division, Almaden Research Center, San Jose, California 95120, USA
[2]Center for Probing the Nanoscale, Stanford University, Stanford, California 94305, USA
[3]Department of Applied Physics, Stanford University, Stanford, California 94305, USA
[4]Department of Physics, Stanford University, Stanford, California 94305, USA
[5]Department of Material Science and Engineering, Stanford University, Stanford, California 94305, USA
*e-mail: poggio@stanford.edu

Capacitive detection

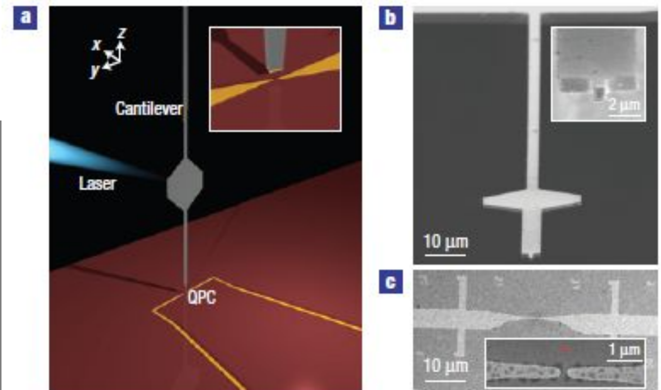

Figure 1 Components and geometry of the experiment. a, Scaled schematic diagram of the experimental set-up. A close-up view of the QPC—with the cantilever in close proximity—is shown in the inset. The laser beam is part of the low-power interferometer used to calibrate displacement measurements made by the QPC. **b**, Scanning electron micrograph of the cantilever and its Au-coated tip (inset). **c**, Scanning electron micrograph of the QPC with a high-resolution view of the active region (inset). The red dot indicates the position of the cantilever tip during the experiment.

$$1\times10^{-12}\, m/\sqrt{Hz}$$

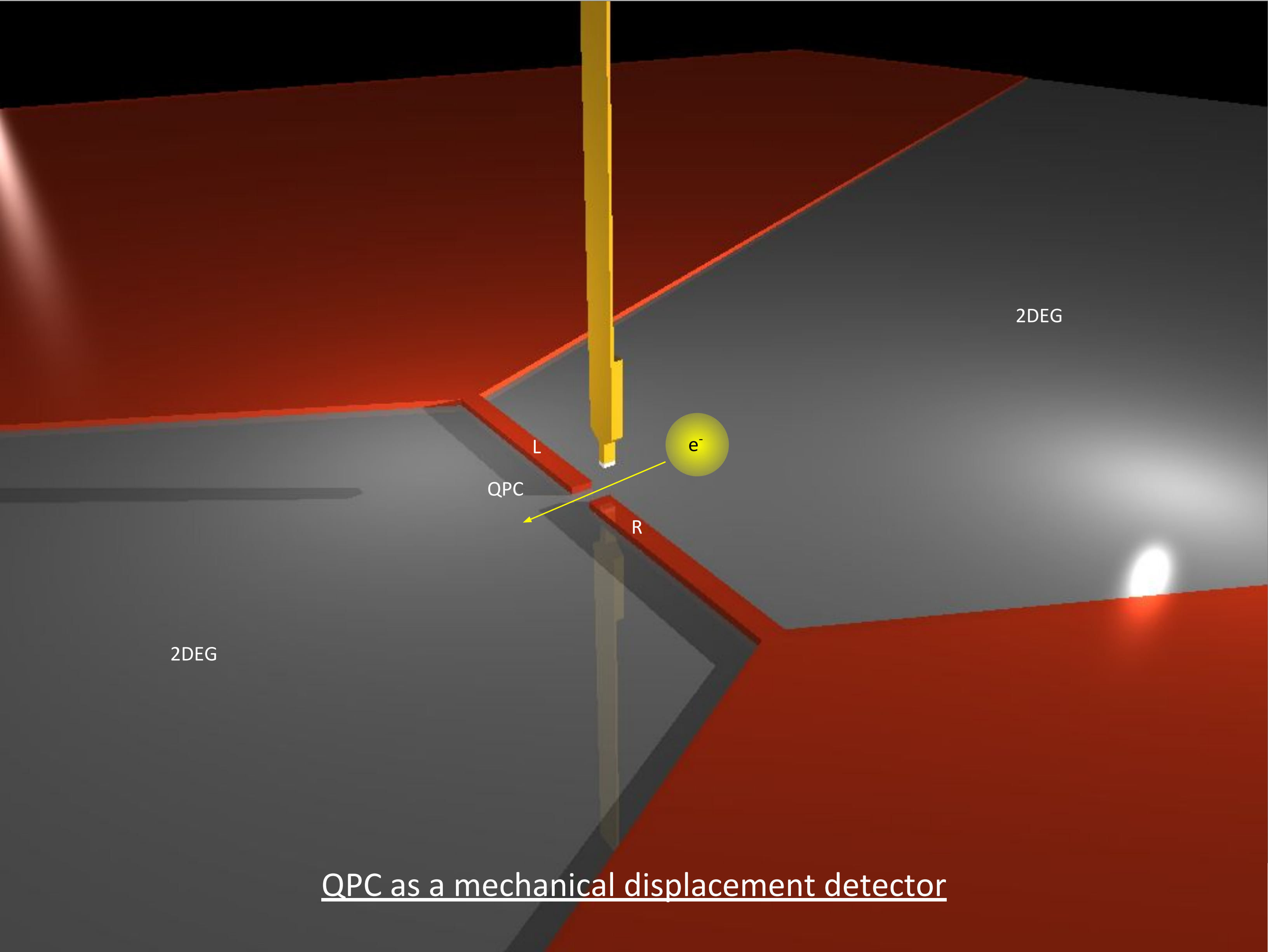
2DEG
L
e-
QPC
R
2DEG
QPC as a mechanical displacement detector

Displacement Measurements

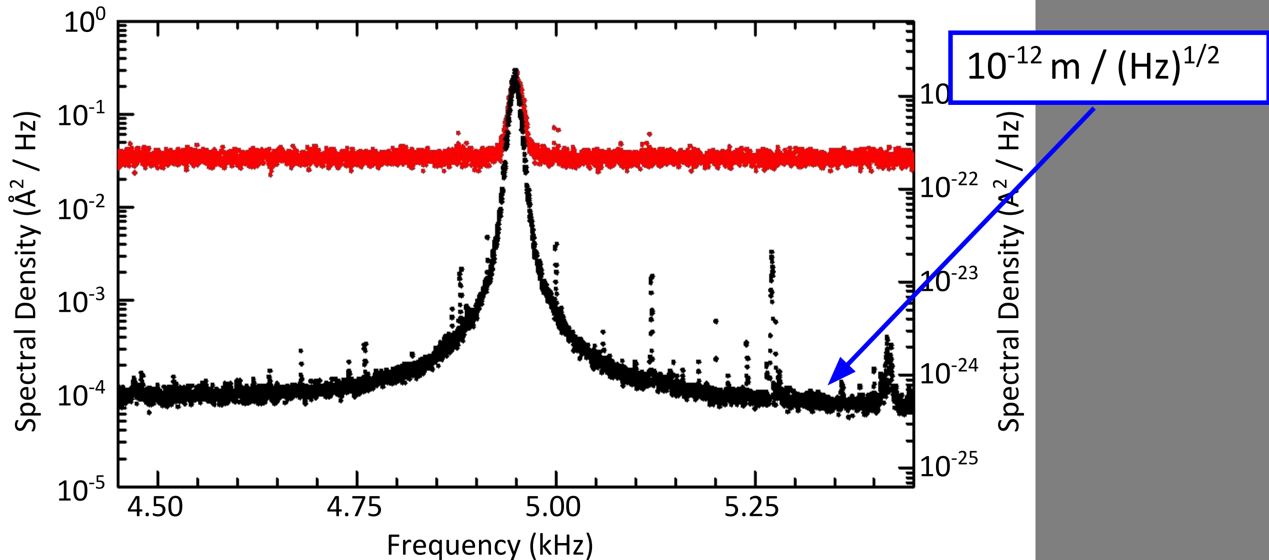

We will now examine in detail displacement detection by optical interferometry.

II. Example: Fiber Interferometer

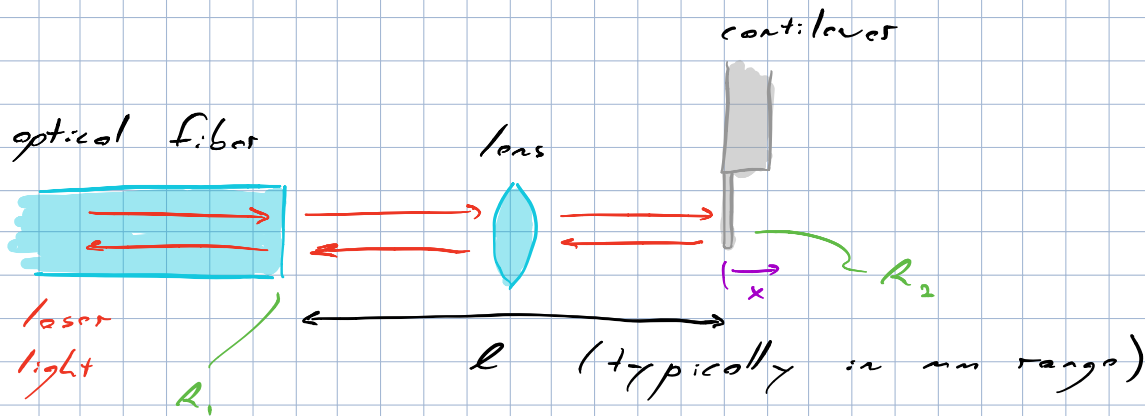

Assume that the reflectivity of the fiber face is R_1 and of the cantilever is R_2. Assume low reflectivities, such that $R_1, R_2 << 1$.

The incident laser power $P_I = E_I^2$, where E_I is the electric field magnitude of the incident laser beam. The power reflected back down the fiber P_R depends on the interference between light reflected at R_1 and R_2:

$$P_R = \left| E_I \sqrt{R_1}\, e^{i\phi_1} + E_I \sqrt{1-R_1}\sqrt{R_2}\sqrt{1-R_1}\, e^{i\phi_2} \right|^2$$

ϕ_1 and ϕ_2 are the phase at R_1 and R_1, respectively.

$$P_R = E_I^2\left[R_1 + (1-R_1)^2 R_2 + 2\sqrt{R_1R_2}\,(1-R_1)\cos(\phi_1-\phi_2)\right]$$

$$P_R = E_I^2\left[R_1 + (1-R_1)^2 R_2 + 2\sqrt{R_1R_2}\,(1-R_1)\cos\left(\frac{4\pi \ell}{\lambda}\right)\right]$$

If $\ell = x_0 + x$

w/ $x_0 = \lambda\left(n + \frac{3}{8}\right)$

for $n = 1, 2, 3, \ldots$, then:

$$P_R = E_I^2\left[R_1 + (1-R_1)^2 R_2 + 2\sqrt{R_1R_2}\,(1-R_1)\sin\left(\frac{4\pi x}{\lambda}\right)\right]$$

Now, let's ignore higher orders of R_1 and R_2:

$$P_R \approx E_I^2\left[R_1 + R_2 + 2\sqrt{R_1R_2}\,\sin\left(\frac{4\pi x}{\lambda}\right)\right]$$

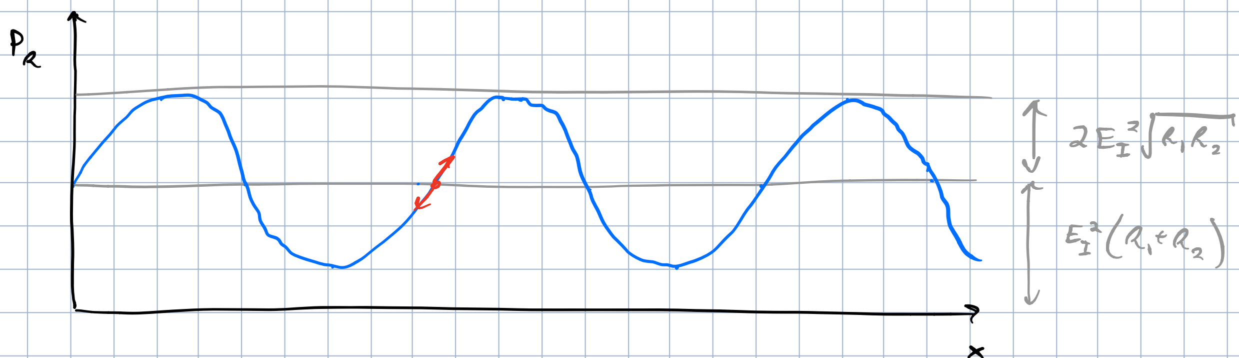

Visibility: $\frac{\text{Amplitude}}{\text{Average}} = \frac{2\sqrt{R_1R_2}}{R_1+R_2}$

Maximum for $R_1 = R_2$ and $R_1, R_2 \to 1$

For $x \ll \lambda$:

$$P_R \approx E_I^2\left[R_1 + R_2 + \frac{8\pi}{\lambda}\sqrt{R_1R_2}\,x\right]$$

For small displacements this is a proportional detector with efficiency :

$$\epsilon \left\{ \frac{8\pi P_I \sqrt{R_1 R_2}}{\lambda} \quad \left[\frac{W}{m} \right] \right.$$

This optical power in Watts is then transformed into an electric current by a photodiode with efficiency S, such that $I_{PD} = S P_R$. The main sources of noise will be electronic noise I_e, shot noise I_{shot}, and mechanical vibration noise I_m.

$$I_e \propto \text{constant}$$

constant current noise independent of optical power

$$I_m = S \epsilon x_{noise} \propto P_I$$

mechanical vibrations

proportional to incident power

Aside : Shot Noise

If the electron arrival events N making up a current are uncorrelated, then they are governed by a Poisson distribution (mean = variance).

- Avg. current : $\langle I \rangle = K e$

- Avg. number of electron arrivals in τ : $\langle n \rangle = K \tau$

- Variance : $\langle n^2 \rangle - \langle n \rangle^2 = \langle n \rangle$

Poissonian

$\therefore$

$$\langle I \rangle = \frac{e}{\tau} \langle n \rangle$$

$$\langle I^2 \rangle = \left\langle \left(\frac{n e}{\tau} \right)^2 \right\rangle = \frac{e^2}{\tau^2} \langle n^2 \rangle$$

$$\langle \Delta I^2 \rangle = \langle I^2 \rangle - \langle I \rangle^2 = \frac{e^2}{\tau^2} \left(\langle n^2 \rangle - \langle n \rangle^2 \right)$$

$$\langle \Delta I^2 \rangle = \frac{e^2}{\tau^2} \langle n \rangle = \frac{e}{\tau} \langle I \rangle$$

$$\Delta I = \sqrt{\frac{e}{\tau} \langle I \rangle}$$

If we consider a bandwidth $\Delta f = \frac{1}{2\tau}$ for an averaging filter and $I = \langle I \rangle$, then :

$$I_{shot} = \sqrt{2 e I \Delta f}$$

So the current shot noise in our photo-detector will depend on the photodiode current I_{PD}:

$$I_{shot} = \sqrt{2e\, I_{PD}\, \Delta f} = \sqrt{2e\, S P_R\, \Delta f}$$

$$I_{shot} \propto \sqrt{P_R} \propto \sqrt{P_I}$$

The signal-to-noise ratio (SNR) of our displacement detection will depend on what kind of noise dominates.

<u>I_e dominates:</u>

$$SNR = \frac{I_{sig}}{I_{noise}} = \frac{S\,\epsilon\, x_{sig}}{I_e}$$

$$SNR = \frac{8\pi}{\lambda}\sqrt{R_1 R_2} \cdot \frac{S P_I}{I_e}\, x_{sig}$$

$$SNR \propto P_I$$ ← linear w/ laser power

<u>I_n dominates:</u>

$$SNR = \frac{I_{sig}}{I_{noise}} = \frac{S\,\epsilon\, x_{sig}}{S\,\epsilon\, x_{noise}}$$

$$SNR = \frac{x_{sig}}{x_{noise}}$$ ← independent of laser power

I_{shot} dominates :

$$SNR = \frac{I_{sig}}{I_{noise}} = \frac{S \epsilon x_{sig}}{\sqrt{2eSP_R \Delta f}}$$

$$SNR \propto \frac{P_I}{\sqrt{P_I}} \propto \sqrt{P_I}$$ ← dependent on square root of laser power

Therefore, the type of limiting noise can be discerned by the dependence of SNR on laser power P_I. Ideally, shot noise dominates the noise, as it is a fundamentally unavoidable source of noise.

In shot noise limit, the ultimate noise floor of the detector is given by :

$$I_{sig} = I_{shot}$$

$$S \epsilon x_{shot} = \sqrt{2eSP_R \Delta f}$$

$$S \frac{8\pi}{\lambda} P_I \sqrt{R_1 R_2}\, x_{shot} = \sqrt{2eSP_I(R_1 + R_2)\Delta f}$$

Shot-noise floor for interferometric detection ↗

$$x_{shot} = \frac{\lambda}{8\pi} \sqrt{\frac{2e\Delta f}{SP_I}} \cdot \sqrt{\frac{R_1 + R_2}{R_1 R_2}}$$

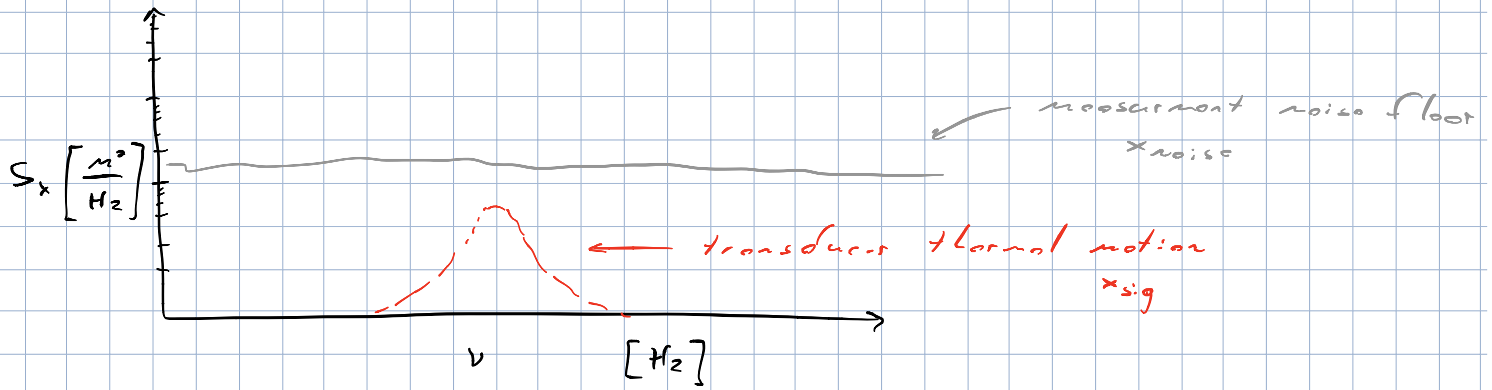

Increase P_I . . .

$$SNR = \frac{x_{sig}}{x_{noise}} \propto \sqrt{P_I}$$

For shot-noise limit

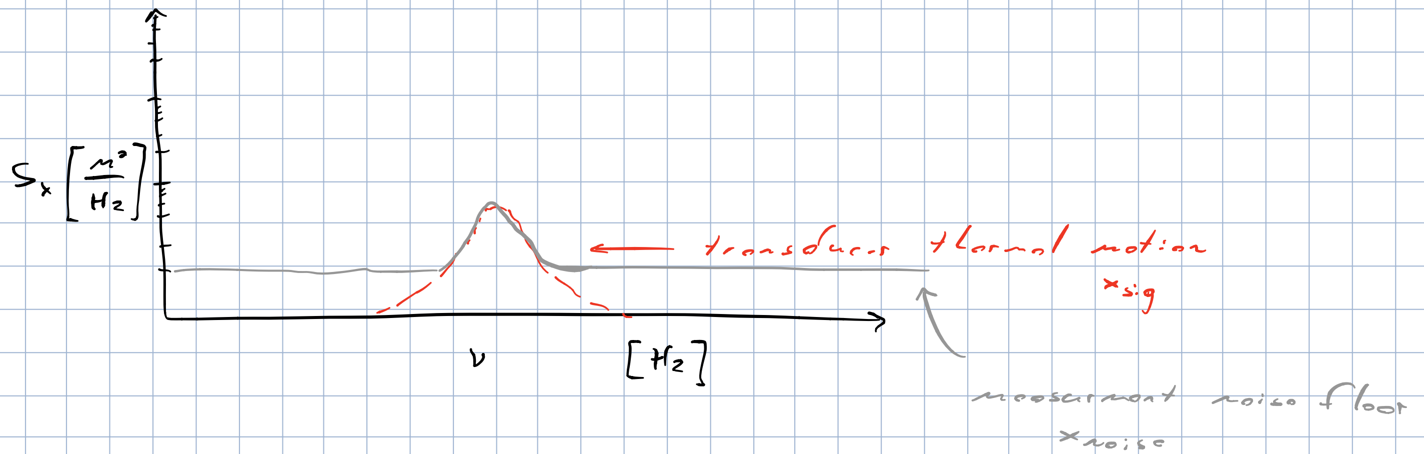

We are interested in improving the fiber-optic interferometer used to sense the displacement of our cantilever. At the moment we have a low-finesse interferometer operated at low power at 1550 nm. We typically operate with between 20 and 100 nW of incident power and we are limited by the detector shot noise rather than by electronic noise. At temperatures below 1 K, energy from laser light absorbed by the Si cantilever is enough to heat the cantilever above the bath temperature. Therefore, we would like to both lower the noise floor of the interferometer (improve it's resolution) and lower the incident power in order to prevent cantilever heating.

Following the reasoning explained in D. Rugar et al. [Rev. Sci. Instrum. 59, 2337 (1988)], we can calculate the noise floor of such a low-finesse, low-power interferometer for 20nW incident power at 1550 nm in $m/\sqrt{Hz}$:

In[12]:=
```
λ = 1550 * 10^-9; ec = 1.602 * 10^-19; S = .4; Pav = 20 * 10^-9;
```

$$\text{Anoise} = \frac{\lambda}{2\pi}\sqrt{\frac{ec}{2\,S\,Pav}}$$

Out[13]= 7.8059×10^{-13}

Note $P_{av} = P_I (R_1 + R_2)$.

Here, $R_1 = R_2$.

The above applies in the case where the effective reflectivities from the cantilever and the fiber are equal. This simplistic treatment of the problem is valid as long as these reflectivities are low or the finesse of the cavity is small. In other words, this model describes the case where light makes only one round-trip in the fiber-cantilever cavity.

For cavities with higher finesse, we must consider multiple reflections, i.e. we must treat the cavity as a Fabry-Perot cavity. Assuming that the fiber surface and the cantilever and perfectly parallel and ignoring losses, we can plot the fraction of the incident power which is reflected as a function of the cavity length:

III. Interferometric Detection in Fabry-Perot Limit

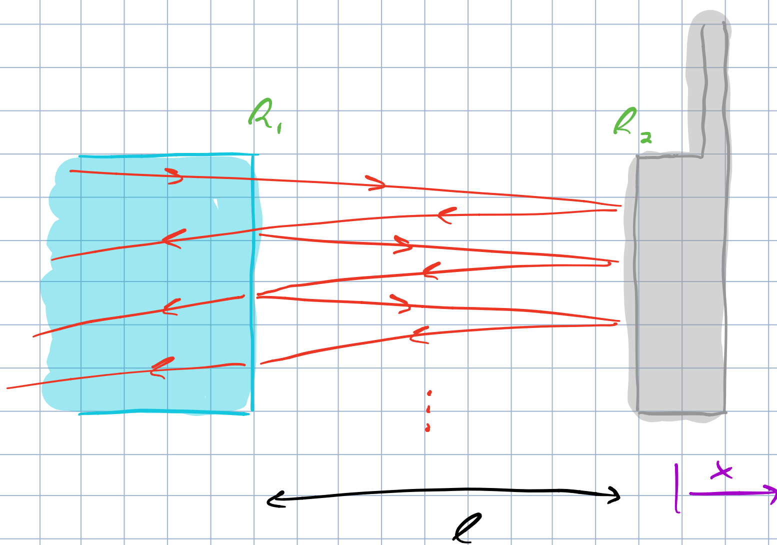

Consider large R_1 and R_2, where multiple reflections cannot be ignored.

$$P_I = E_I^2 \quad , \quad P_R = |E_R|^2 \quad , \quad P_T = |E_T|^2$$

$$E_T = E_I \left[\sqrt{T_1}\sqrt{T_2}\, e^{i\frac{2\pi \ell}{\lambda}} + \sqrt{T_1}\sqrt{R_2}\sqrt{R_1}\sqrt{T_2}\, e^{i\frac{6\pi \ell}{\lambda}} + \ldots \right]$$

$$E_T = E_I \sqrt{T_1 T_2}\, e^{i\frac{2\pi \ell}{\lambda}} \underbrace{\left[\sum_{n=0}^{\infty} \left(\sqrt{R_1 R_2}\, e^{i\frac{4\pi \ell}{\lambda}} \right)^n \right]}_{\frac{1}{1 - \sqrt{R_1 R_2}\, e^{i\frac{4\pi \ell}{\lambda}}}}$$

$$E_T = E_I \frac{\sqrt{T_1 T_2}\, e^{i\frac{2\pi \ell}{\lambda}}}{1 - \sqrt{R_1 R_2}\, e^{i\frac{4\pi \ell}{\lambda}}}$$

$$P_T = |E_T|^2 = E_I^2 \frac{T_1 T_2}{1 + R_1 R_2 - 2\sqrt{R_1 R_2} \underbrace{\cos\left(\frac{4\pi \ell}{\lambda}\right)}_{1 - 2\sin^2\left(\frac{2\pi \ell}{\lambda}\right)}}$$

$$P_T = |E_T|^2 = P_I \frac{(1-R_1)(1-R_2)}{(1-\sqrt{R_1R_2})^2 + 4\sqrt{R_1R_2}\sin^2\left(\frac{2\pi\ell}{\lambda}\right)}$$

$$P_T = P_I \frac{\frac{(1-R_1)(1-R_2)}{(1-\sqrt{R_1R_2})^2}}{1 + \underbrace{\frac{4\sqrt{R_1R_2}}{(1-\sqrt{R_1R_2})^2}}_{F \text{ (finesse)}}\sin^2\left(\frac{2\pi\ell}{\lambda}\right)}$$

$$P_R = P_I - P_T$$

$$P_R = P_I \left[1 - \frac{\frac{(1-R_1)(1-R_2)}{(1-\sqrt{R_1R_2})^2}}{1 + F\sin^2\left(\frac{2\pi\ell}{\lambda}\right)} \right]$$

← Depends sensitively on cavity length ℓ

For small x around x_0:

$$P_R = P_R(x_0) + \frac{\partial P_R}{\partial \ell}(x_0) \cdot x$$

$$\therefore \quad I_{sig} \approx S \frac{\partial P_R}{\partial \ell}(x_0) \cdot x_{sig}$$

In the shot noise limit:

$$I_{shot} \approx \sqrt{2 e S P_R(x_0) \Delta f}$$

$$\therefore \quad I_{sig} = I_{shot}$$

$$S \frac{\partial P_R}{\partial \ell}(x_0) \cdot x_{shot} = \sqrt{2 e S P_R(x_0) \Delta f}$$

$$x_{shot} = \sqrt{\frac{2 e P_R(x_0) \Delta f}{S}} \frac{1}{\frac{\partial P_R}{\partial \ell}(x_0)}$$

In[14]:=
```
λ = 1550 * 10^-9; R1 = .5; R2 = .5; n = 1;
```

$$F = \frac{4\sqrt{R1\,R2}}{\left(1-\sqrt{R1\,R2}\right)^2}$$

$$\text{Plot}\left[1-\frac{\frac{(1-R1)\,(1-R2)}{\left(1-\sqrt{R1\,R2}\right)^2}}{1+F\,\text{Sin}\left[\frac{2\pi n l}{\lambda}\right]^2},\ \{l,\ 0,\ 2000*10^{-9}\},\ \text{ImageSize}\to 500,\ \text{PlotRange}\to\{0,\ 1\}\right]$$

Out[15]= 8.

Out[16]=

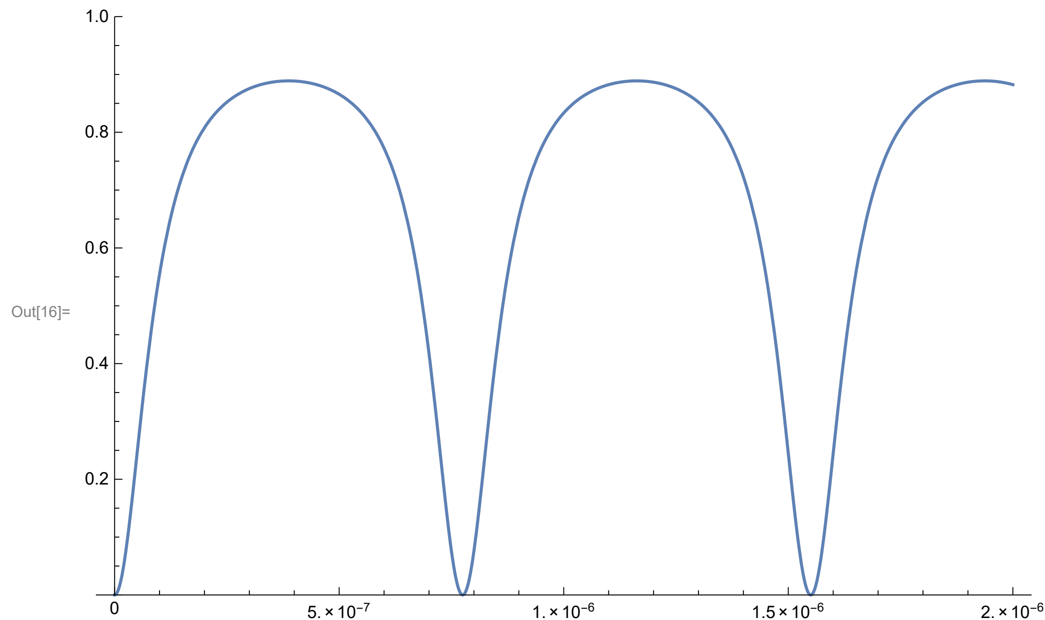

In the above case, R1 and R2 are the reflectivity of the fiber and the cantilever respectively. In the low-finesse limit, as shown below, we can compare the two models and we see that they yeild similar results:

In[17]:=

$$\lambda = 1550 * 10^{-9};\ R1 = .1;\ R2 = .1;\ n = 1;$$

$$F = \frac{4\sqrt{R1\ R2}}{\left(1 - \sqrt{R1\ R2}\right)^2}$$

$$\text{Plot}\left[\left\{R1 + (1 - R1)^2\, R2 + 2\,(1 - R1)\sqrt{R1\ R2}\ \text{Cos}\left[\frac{4\,\pi\, l}{\lambda} - \text{Pi}\right],\ 1 - \frac{\frac{(1-R1)\,(1-R2)}{\left(1-\sqrt{R1\ R2}\right)^2}}{1 + F\ \text{Sin}\left[\frac{2\,\pi\, n\, l}{\lambda}\right]^2}\right\},\right.$$

$$\left.\{l,\ 0 * 10^{-9},\ \lambda\},\ \text{ImageSize} \to 500,\ \text{PlotRange} \to \{0, 1\},\ \text{PlotStyle} \to \{\text{Hue}[0],\ \text{Hue}[.7]\}\right]$$

Out[18]= 0.493827

Out[19]=

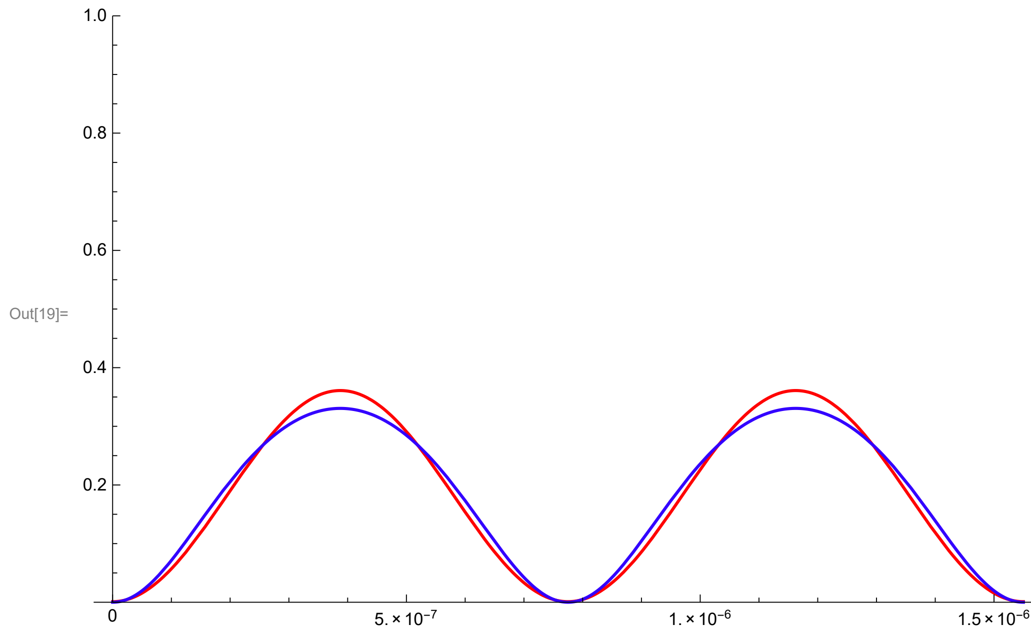

If we improve the reflectivities of the lever and the fiber, then we will have to use the Fabry-Perot model. Let's see how much our noise floor will improve if we improve these reflectivities. Solving for the reflected power from a Fabry-Perot cavity we have $P_r = P\left(1 - \frac{\frac{(1-R1)\,(1-R2)}{\left(1-\sqrt{R1\ R2}\right)^2}}{1 + \frac{4\sqrt{R1\ R2}}{\left(1-\sqrt{R1\ R2}\right)^2}\,\text{Sin}\left[\frac{2\,\pi\, n\, l}{\lambda}\right]^2}\right)$. For small changes in the cantilever displacement ($x << l$), the displacement signal in terms of current will be $I_s = x\, S\, P_r'(l)$. The associated current shot noise will be $I_n = \sqrt{2\, e\, S\, P_r(l)}$. Therefore the rms displacement noise floor is given by $x_n = \frac{\sqrt{2\, e\, S\, P_r(l)}}{S\, P_r'(l)} = \sqrt{\frac{2\, e\, P_r(l)}{S}}\ \frac{1}{P_r'(l)}$. Let's solve for these terms and plot them. Let's also include some absorption α and some current noise.

In[20]:=
```
Clear[λ, R1, R2, n, l, P, α];
```

$$D\left[P\left(1-\frac{\frac{(1-R1)\ (1-R2)\ (1-\alpha)^2}{\left(1-\sqrt{R1\,R2}\right)^2}}{1+\frac{4\sqrt{R1\,R2}}{\left(1-\sqrt{R1\,R2}\right)^2}\,\mathrm{Sin}\left[\frac{2\,\pi\,n\,l}{\lambda}\right]^2}\right),\ \{l,\ 1\}\right]$$

Out[21]=

$$\left(16\,n\,P\,\pi\,(1-R1)\,(1-R2)\,\sqrt{R1\,R2}\,(1-\alpha)^2\,\mathrm{Cos}\left[\frac{2\,l\,n\,\pi}{\lambda}\right]\,\mathrm{Sin}\left[\frac{2\,l\,n\,\pi}{\lambda}\right]\right)\Big/\left(\left(1-\sqrt{R1\,R2}\right)^4\,\lambda\,\left(1+\frac{4\sqrt{R1\,R2}\,\mathrm{Sin}\left[\frac{2\,l\,n\,\pi}{\lambda}\right]^2}{\left(1-\sqrt{R1\,R2}\right)^2}\right)^2\right)$$

In[22]:=
$$\lambda = 1550 * 10^{-9};$$
$$R1 = .3;$$
$$R2 = .3;$$
$$n = 1;$$
$$S = 0.4;$$
$$ec = 1.602 * 10^{-19};$$
$$P = 20 * 10^{-9};$$
$$\alpha = 10^{-2};$$
$$Inoise = 10^{-13};$$

$$\text{LogPlot}\left[\left\{\frac{\sqrt{2\,ec\,S\,P\left(1 - \frac{\frac{(1-R1)\,(1-R2)\,(1-\alpha)^2}{\left(1-\sqrt{R1\,R2}\right)^2}}{1+\frac{4\sqrt{R1\,R2}}{\left(1-\sqrt{R1\,R2}\right)^2}\,\text{Sin}\left[\frac{2\,\pi\,n\,l}{\lambda}\right]^2}\right) + Inoise}}{\text{Abs}\left[S\,P\,\frac{16\,n\,\pi\,(1-R1)\,(1-R2)\,\sqrt{R1\,R2}\,(1-\alpha)^2\,\text{Cos}\left[\frac{2\,l\,n\,\pi}{\lambda}\right]\,\text{Sin}\left[\frac{2\,l\,n\,\pi}{\lambda}\right]}{\left(1-\sqrt{R1\,R2}\right)^4\,\lambda\left(1+\frac{4\sqrt{R1\,R2}\,\text{Sin}\left[\frac{2\,l\,n\,\pi}{\lambda}\right]^2}{\left(1-\sqrt{R1\,R2}\right)^2}\right)^2}\right]}\right\}, \{l, 0 * 10^{-9}, \lambda\},$$
$$\text{ImageSize} \to 700,\ \text{PlotStyle} \to \{\text{Hue}[0], \text{Hue}[.7]\},\ \text{PlotRange} \to \{10^{-16}, 10^{-11}\}\right]$$

Out[23]=

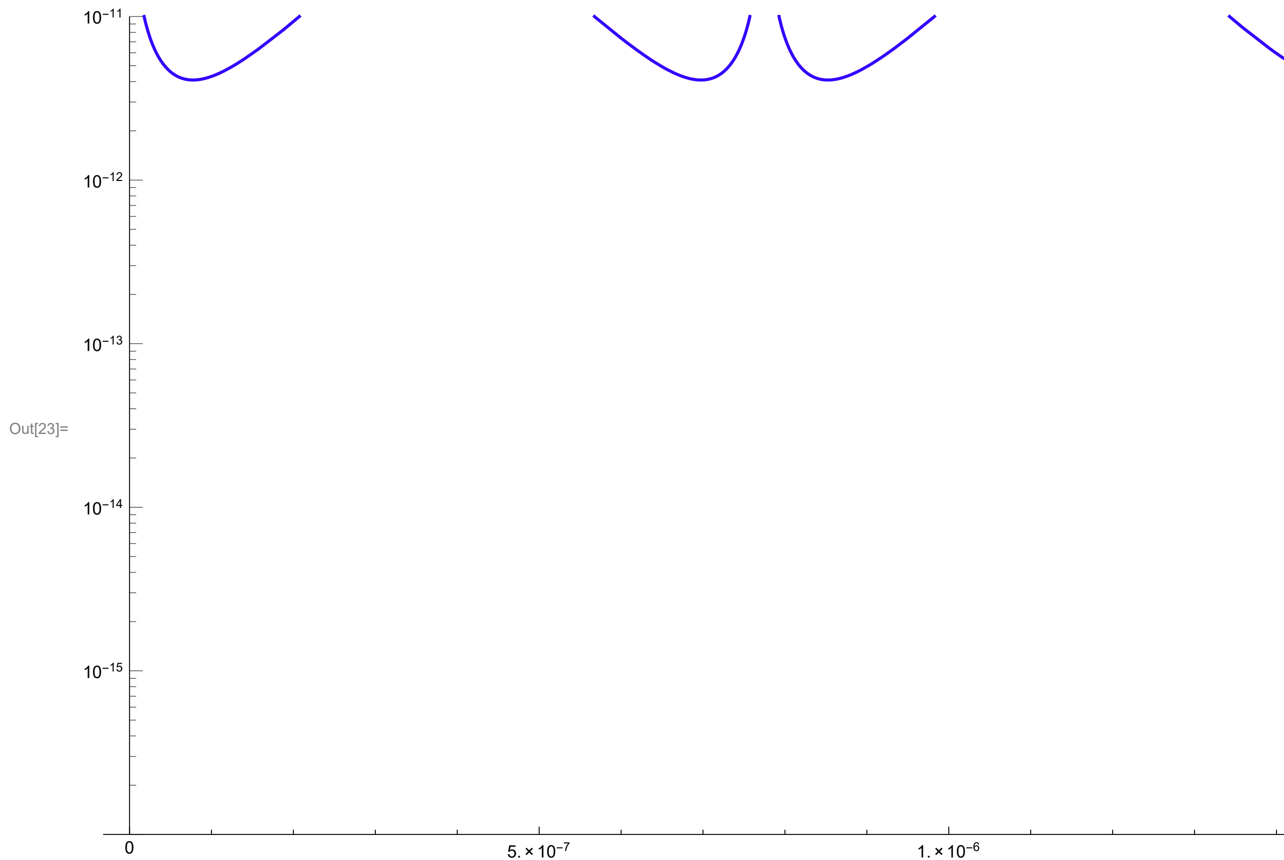

In[24]:=
```
λ = 1550 * 10^-9;
R1 = .75;
R2 = .75;
n = 1;
S = 0.4;
ec = 1.602 * 10^-19;
P = 20 * 10^-9;
α = 10^-2;
Inoise = 10^-13;
```

$$\text{LogPlot}\left[\left\{\frac{\sqrt{2\,\text{ec}\,S\,P\left(1-\frac{\frac{(1-\text{R1})\,(1-\text{R2})\,(1-\alpha)^2}{\left(1-\sqrt{\text{R1 R2}}\right)^2}}{1+\frac{4\sqrt{\text{R1 R2}}}{\left(1-\sqrt{\text{R1 R2}}\right)^2}\text{Sin}\left[\frac{2\pi n l}{\lambda}\right]^2}\right)+\text{Inoise}}}{\text{Abs}\left[S\,P\,\frac{16\,n\,\pi\,(1-\text{R1})\,(1-\text{R2})\sqrt{\text{R1 R2}}\,(1-\alpha)^2\,\text{Cos}\left[\frac{2 l n \pi}{\lambda}\right]\text{Sin}\left[\frac{2 l n \pi}{\lambda}\right]}{\left(1-\sqrt{\text{R1 R2}}\right)^4\lambda\left(1+\frac{4\sqrt{\text{R1 R2}}\,\text{Sin}\left[\frac{2 l n \pi}{\lambda}\right]^2}{\left(1-\sqrt{\text{R1 R2}}\right)^2}\right)^2}\right]}\right\},\ \{l,\ 0*10^{-9},\ \lambda\},$$

ImageSize → 700, PlotStyle → {Hue[0], Hue[.7]}, PlotRange → $\{10^{-16}, 10^{-11}\}$]

Out[25]=

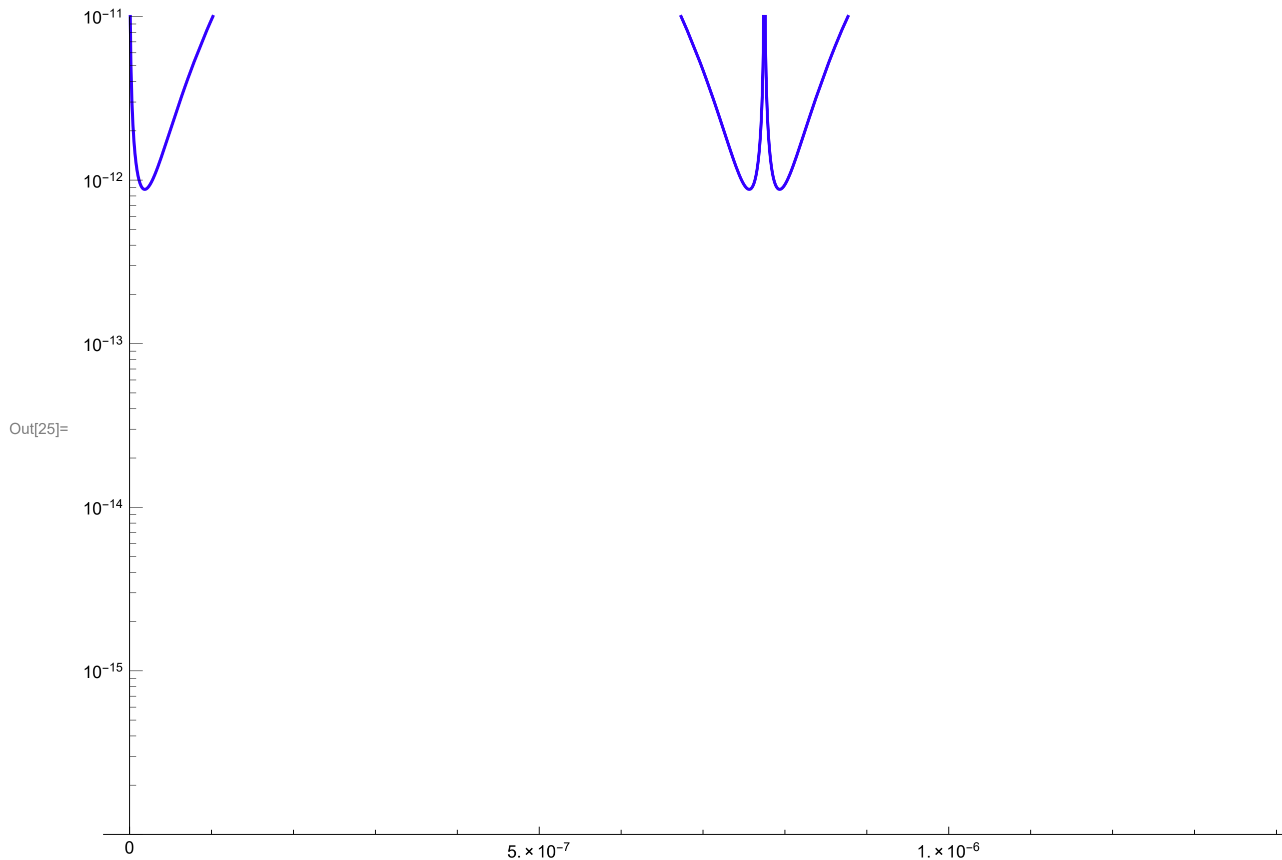

In[26]:=
```
λ = 1550 * 10^-9;
R1 = .95;
R2 = .95;
n = 1;
S = 0.4;
ec = 1.602 * 10^-19;
P = 20 * 10^-9;
α = 10^-2;
Inoise = 10^-13;
```

$$\text{LogPlot}\left[\left\{\frac{\sqrt{2\,\text{ec}\,\text{S}\,\text{P}\left(1-\frac{\frac{(1-\text{R1})\,(1-\text{R2})\,(1-\alpha)^2}{\left(1-\sqrt{\text{R1 R2}}\right)^2}}{1+\frac{4\sqrt{\text{R1 R2}}}{\left(1-\sqrt{\text{R1 R2}}\right)^2}\,\text{Sin}\left[\frac{2\pi\,\text{n}\,\text{l}}{\lambda}\right]^2}\right)+\text{Inoise}}}{\text{Abs}\left[\text{S}\,\text{P}\,\frac{16\,\text{n}\,\pi\,(1-\text{R1})\,(1-\text{R2})\,\sqrt{\text{R1 R2}}\,(1-\alpha)^2\,\text{Cos}\left[\frac{2\,\text{l}\,\text{n}\,\pi}{\lambda}\right]\,\text{Sin}\left[\frac{2\,\text{l}\,\text{n}\,\pi}{\lambda}\right]}{\left(1-\sqrt{\text{R1 R2}}\right)^4\,\lambda\left(1+\frac{4\sqrt{\text{R1 R2}}\,\text{Sin}\left[\frac{2\,\text{l}\,\text{n}\,\pi}{\lambda}\right]^2}{\left(1-\sqrt{\text{R1 R2}}\right)^2}\right)^2}\right]}\right\},\ \{\text{l},\ 0*10^{-9},\ \lambda\},$$

```
ImageSize → 700, PlotStyle → {Hue[0], Hue[.7]}, PlotRange → {10^-16, 10^-11}]
```

Out[27]=

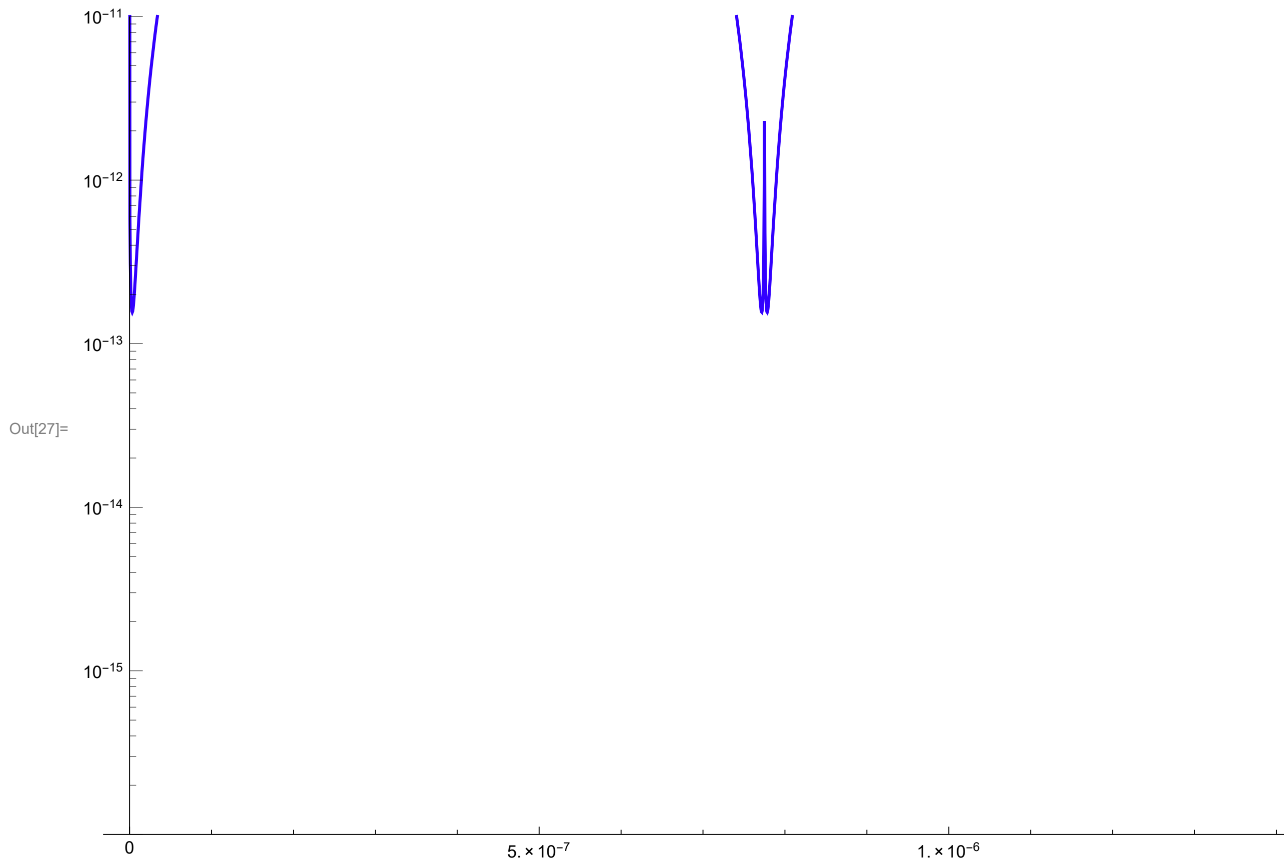

In[28]:=
```
λ = 1550 * 10^-9;
R1 = .995;
R2 = .995;
n = 1;
S = 0.4;
ec = 1.602 * 10^-19;
P = 20 * 10^-9;
α = 10^-2;
Inoise = 10^-13;
```

$$\text{LogPlot}\Big[\Big\{\frac{\sqrt{2\,\text{ec}\,S\,P\left(1-\frac{\frac{(1-\text{R1})\,(1-\text{R2})\,(1-\alpha)^2}{\left(1-\sqrt{\text{R1 R2}}\right)^2}}{1+\frac{4\sqrt{\text{R1 R2}}}{\left(1-\sqrt{\text{R1 R2}}\right)^2}\,\text{Sin}\left[\frac{2\pi n l}{\lambda}\right]^2}\right)}+\text{Inoise}}{\text{Abs}\left[S\,P\,\frac{16\,n\,\pi\,(1-\text{R1})\,(1-\text{R2})\,\sqrt{\text{R1 R2}}\,(1-\alpha)^2\,\text{Cos}\left[\frac{2 l n\pi}{\lambda}\right]\,\text{Sin}\left[\frac{2 l n\pi}{\lambda}\right]}{\left(1-\sqrt{\text{R1 R2}}\right)^4\lambda\left(1+\frac{4\sqrt{\text{R1 R2}}\,\text{Sin}\left[\frac{2 l n\pi}{\lambda}\right]^2}{\left(1-\sqrt{\text{R1 R2}}\right)^2}\right)^2}\right]}\Big\},\ \{l,\ 0*10^{-9},\ \lambda\},$$

```
 ImageSize → 700, PlotStyle → {Hue[0], Hue[.7]}, PlotRange → {10^-16, 10^-11}]
```

Out[29]=

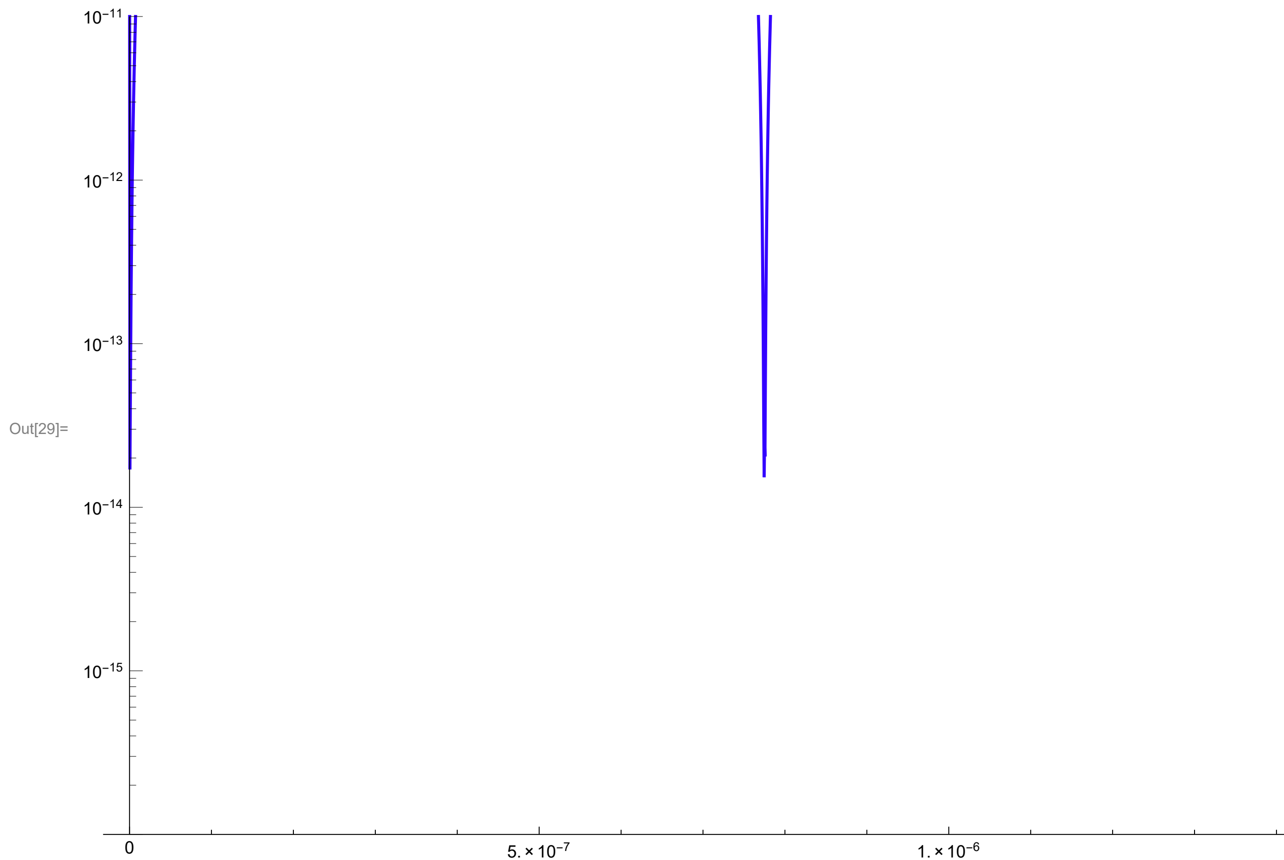

We have considered cases where R1 = R2 since this condition minimizes the noise floor for any given λ as shown below:

In[30]:=
```
λ = 1550 * 10^-9;
n = 1;
S = 0.4;
ec = 1.602 * 10^-19;
P = 20 * 10^-9;
Clear[R1, R2];
l = λ / 1000;
```

$$\text{Plot3D}\left[\text{Log}\left[10, \frac{\sqrt{2\,\text{ec}\,S\,P\left(1 - \frac{\frac{(1-R1)(1-R2)}{\left(1-\sqrt{R1\,R2}\right)^2}}{1+\frac{4\sqrt{R1\,R2}}{\left(1-\sqrt{R1\,R2}\right)^2}\text{Sin}\left[\frac{2\pi n l}{\lambda}\right]^2}\right)}}{\text{Abs}\left[S\,P\,\frac{16\,n\,\pi\,(1-R1)\,(1-R2)\,\sqrt{R1\,R2}\,\text{Cos}\left[\frac{2\,l\,n\,\pi}{\lambda}\right]\text{Sin}\left[\frac{2\,l\,n\,\pi}{\lambda}\right]}{\left(1-\sqrt{R1\,R2}\right)^4\lambda\left(1+\frac{4\sqrt{R1\,R2}\,\text{Sin}\left[\frac{2\,l\,n\,\pi}{\lambda}\right]^2}{\left(1-\sqrt{R1\,R2}\right)^2}\right)^2}\right]}\right], \{R1, 0.01, .99\},$$

```
{R2, 0.01, .99}, ImageSize → 500, PlotPoints → 300, Mesh → False]
```

Out[31]=

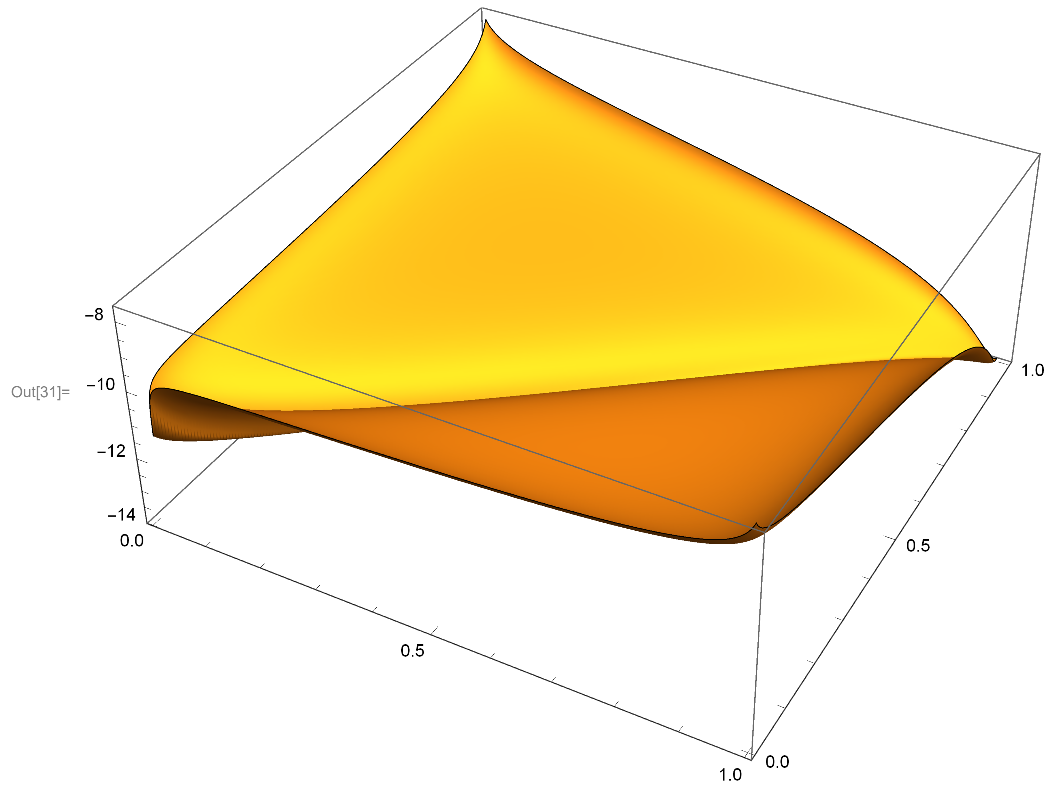

In[32]:=

```
λ = 1550/10^9;
n = 1;
S = 0.4`;
ec = 1.602`/10^19;
P = 20/10^9;
Clear[R1, R2];
l = λ/1000
```

$$\text{ContourPlot}\left[\text{Log}\left[10, \frac{\sqrt{2\,\text{ec}\,S\,P\left(1-\frac{(1-R1)\,(1-R2)}{\left(1-\sqrt{R1\,R2}\right)^2\left(1+\frac{\left(4\sqrt{R1\,R2}\right)\text{Sin}\left[\frac{2\pi n l}{\lambda}\right]^2}{\left(1-\sqrt{R1\,R2}\right)^2}\right)}\right)}}{\text{Abs}\left[\frac{S\,P\left(16\,n\,\pi\,(1-R1)\,(1-R2)\,\sqrt{R1\,R2}\,\text{Cos}\left[\frac{2\,l\,n\,\pi}{\lambda}\right]\text{Sin}\left[\frac{2\,l\,n\,\pi}{\lambda}\right]\right)}{\left(1-\sqrt{R1\,R2}\right)^4\lambda\left(1+\frac{4\sqrt{R1\,R2}\,\text{Sin}\left[\frac{2\,l\,n\,\pi}{\lambda}\right]^2}{\left(1-\sqrt{R1\,R2}\right)^2}\right)^2}\right]}\right],\right.$$

```
{R1, 0.01`, 0.99`}, {R2, 0.01`, 0.99`}, ImageSize → 500, ContourStyle → Automatic]
```

Out[33]=

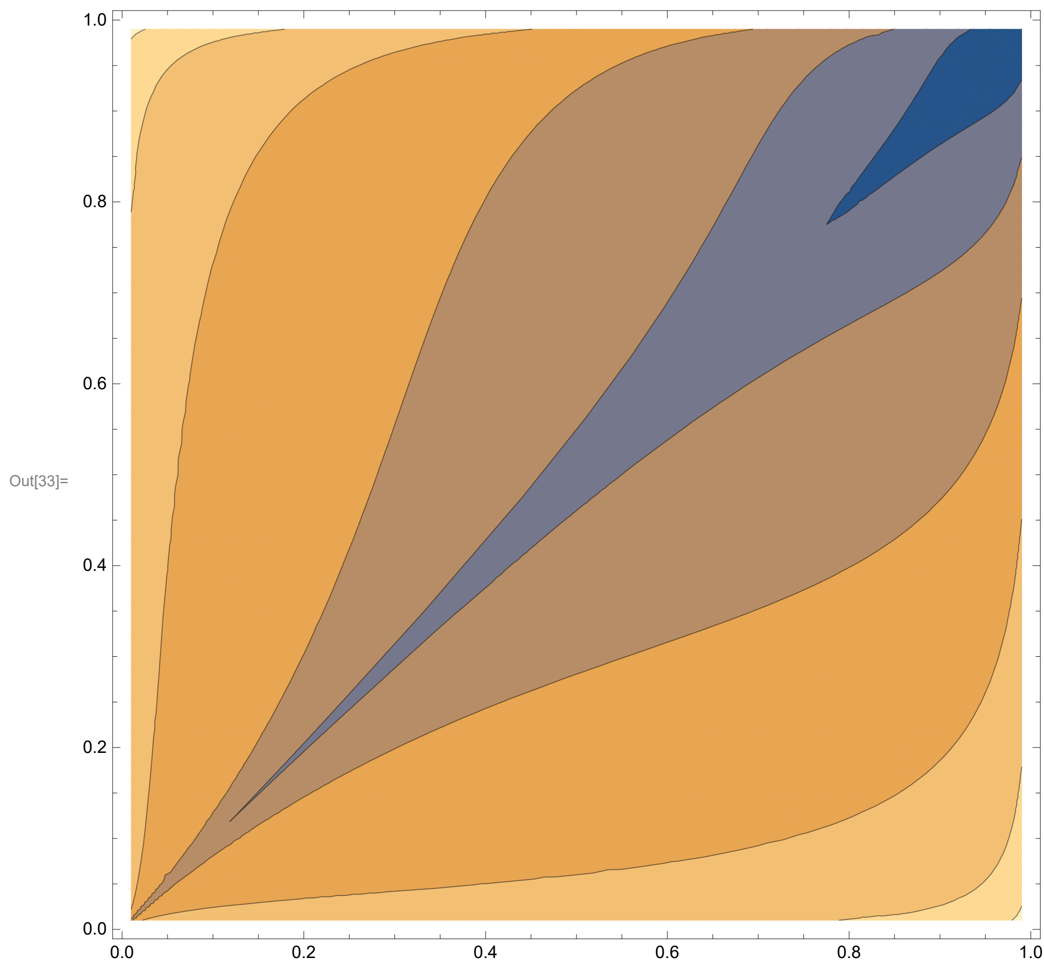

From these calculations we can conclude that increasing the reflectivity -- and therefore the finesse -- of our cavity will improve our displacement detection noise.

For 30% reflectivity we have 5 x 10^{-13}m$\Big/\sqrt{\text{Hz}}$ (similar to current conditions)

For 75% reflectivity we have 1 x 10^{-13}m$\Big/\sqrt{\text{Hz}}$

For 95% reflectivity we have 2 x 10^{-14}m$\Big/\sqrt{\text{Hz}}$

For 99.5% reflectivity we have 2 x 10^{-15}m$\Big/\sqrt{\text{Hz}}$